Available online at www.sciencedirect.com
SCIENCE DIRECT®
Physica A 341 (2004) 482–494
PHYSICA A
www.elsevier.com/locate/physa

Non-Turing stripes and spots: a novel mechanism for biological cell clustering

Wei Zeng[a], Gilberto L. Thomas[b,1], James A. Glazier[a,*]

[a] *Department of Physics and Biocomplexity Institute, Indiana University, Swain Hall West 159, 727 East 3rd Street, Bloomington, IN 47405-7105, USA*

[b] *Department of Physics and Interdisciplinary Center for the Study of Biocomplexity, 313 Nieuwland, University of Notre Dame, Notre Dame, IN 46556-5670, USA*

Received 19 August 2003; received in revised form 6 February 2004

Abstract

A classical model for developmental patterning invokes a chemical 'prepattern' which cells read out as developmental instructions. The 'prepattern' arises from the Turing Instability of two reacting and diffusing chemicals, an 'activator' and an 'inhibitor.' We propose a novel developmental mechanism, based on cell–cell adhesion and cell–extracellular matrix (ECM) adhesion, which depends only on biological mechanisms and chemicals shown experimentally to be significant during patterning. In our model, condensation results from random cell diffusion biased by preferential attachment of cells to ECM and enhanced local cell–cell adhesion. We implement a two-dimensional Cellular Potts Model (CPM) simulation of condensation to explore this mechanism and discuss the parameter dependencies of the patterns. The simulation reproduces much of the density-dependent phenomenology of in vitro biological cell clustering during the developmental process of chick limb precartilage mesenchymal condensation. We study pattern formation in our model and compare it to the standard Turing mechanism. The mechanism should apply to other condensation processes besides limb chondrogenesis in vivo. The existance of an overlooked and simple mechanism which explains the observed phenomenology better than the classical picture is genuinely surprising.

PACS: 87.18.Ed; 87.18.La; 87.17.Aa

Keywords: Cell adhesion; Extracellular matrix (ECM); Cellular Potts Model (CPM); Precartilage mesenchymal condensation; Limb chondrogenesis

* Corresponding author.
E-mail address: glazier@indiana.edu (J.A. Glazier).

[1] Permanent address: Instituto de Física, Universidade Federal do Rio Grande do Sul, Porto Alegre, RS 91501-970, Brazil.

0378-4371/$ - see front matter
doi:10.1016/j.physa.2004.03.089

1. Introduction

Mesenchymal condensation, in which *mesenchymal* cells (i.e., cells that form part of the bulk tissues rather than the epithelial surfaces) *condense* (i.e., coalesce) into compact clusters) is the earliest stage of organogenesis and is crucial to the development of skeletal and other mesenchymal tissues (e.g. cartilage, kidney, lung, etc.). The morphology of the condensations lays down the shape of future organs [1,2]. In this paper we propose a novel developmental mechanism for mesenchymal condensation, based on cell–cell and cell–extracellular matrix (*ECM*, the loosely structured noncellular scaffolding which surrounds and supports the cells) adhesion. We use it to explain the clustering and differentiation of a previously dispersed population of mesenchymal cells during precartilage mesenchymal condensation in chick limb *chondrogenesis* (bone patterning and formation), a specific case of the more general developmental phenomenon. We compare the results to those the Turing mechanism produces, which Newman and others have proposed as explaining mesenchymal condensation [3].

Turing proposed a reaction-diffusion mechanism for biological pattern formation in 1952 [4] and patterns similar to Turing-type also occur in certain chemical reactions [5]. A Turing pattern results spontaneously from the reaction and diffusion of two initially homogeneous chemical substances: *activator* (A) and *inhibitor* (I), provided that I diffuses faster than A. A promotes the production of both A and I, while I inhibits the production of A. A zone of elevated concentration of A increases the concentration of I over a larger area, inhibiting A in the surrounding region and leading to an inhomogeneous spatial distribution of A and I. Basic patterns include spots, simple stripes and labyrinths, while fine tuning the parameters can produce a whole zoo of patterns.

Many explanations of biological patterning invoke the Turing mechanism, e.g. for the patterning of animal coats, feather buds and fish skin [6,7]. In this class of models, the standard Turing mechanism establishes a chemical pre-pattern and cells interpret the pattern by differentiating only where the chemical (morphogen) concentration is above a certain threshold [1,2]. The Turning model is incomplete in several respects: the huge inventory of molecules involved in morphogenesis includes very few which behave like classical activators or inhibitors. No activators or inhibitors are known for mesenchymal condensation. The cells do not influence the static chemical 'prepattern', making development into a slave process, while real cells actively reshape their environment. The model requires an additional process (e.g. selective differentiation or chemotaxis) to lock in the labile prepattern. These problems led us to look for a simple patterning mechanism that could reproduce the basic Turing patterns using only biological mechanisms proved experimentally to act during mesenchymal condensation.

2. Biology

Recent experiments show that extracellular matrix molecules and membrane-bound cell adhesion molecules, such as *fibronectin* (a sticky protein in the ECM) and N-CAM (a cell–cell adhesion molecule) play an important role in initiating cell clustering during precartilage mesenchymal condensation [8].

Precartilage mesenchymal cells are swarming cells that secrete a variety of complex molecules which form the ECM, the porous environment which is largely responsible for the mechanical integrity of connective tissues and which provides a substrate for cell migration [9]. Of the many ECM components, we focus here on the adhesive nondiffusing molecule fibronectin. Mesenchymal cells prefer to attach to fibronectin and can move up gradients in fibronectin concentration, a phenomenon called "haptotaxis." Besides serving as a "railway" guiding cell migration, fibronectin also interacts with integrins on the cell surface and triggers intracellular signaling cascades which affect cell properties and gene expression [10]. Fibronectin expression and synthesis increase 4-5-fold at the onset of condensation at precartilage mesenchymal condensation sites in vivo and in vitro [11]. The signaling molecule TGF-β plays a role in the regulation of fibronectin production [12]. TGF-β is a candidate for the 'activator' the reaction–diffusion model of biological patterning requires [13]. Intensive searches have also suggested a possible 'inhibitor' [14], but so far neither search has clearly identified the activator or the inhibitor.

Condensing precartilage mesenchymal cells can also adhere to each other directly through transmembrane adhesion molecules, such as N-CAMs and N-cadherins. Condensing cells express N-cadherin during chondrogenesis (cartilage formation) in the developing limb bud in vivo and in limb bud micromass culture in vitro. The time of maximal expression of *N*-cadherin corresponds to the period of active precartilage mesenchymal condensation [15]. Experiments which induce over- or under-expression of N-CAM both in vivo and in vitro suggest that *N*-CAM also promotes mesenchymal condensation [16].

Integrins, another class of cell adhesion molecule, attach primarily to proteins bound to the extracellular matrix [17]. Binding of fibronectin to integrin can promote cadherin-mediated cell–cell adhesion by upregulating cadherin production [18]. Changing the extracellular environment [19] and changing cell adhesiveness can influence the pattern of condensation in vitro [20].

Taken together, the experiments suggest that attachment of mesenchymal cells to ECM and the resulting enhanced local cell–cell adhesion suffice to initiate and maintain cell clustering during precartilage mesenchymal condensation.

We focus on in vitro micromass experiments which produce patterns similar to those in vivo. Micromass cultures avoid the complicating effects of other morphogens (e.g. the FGFs, Shh, and others) and allow direct two-dimensional visualization, making comparison to simulations easier.

3. Methods

We implement a Cellular Potts Model (CPM) [21,22] simulation on a two-dimensional lattice. The two-dimensional model reflects the quasi-two-dimensional micromass experiment. Our simulation produces a density dependent morphology which we compare to experimental data. We also discuss possible extensions to our model to study the formation of pattern and shape during limb chondrogenesis.

Glazier and Graner introduced the CPM to describe surface-energy-driven biological processes at the cellular scale such as two-cell-type cell sorting [21,22]. The CPM

represents the spatial distribution of N cells, indexed by σ, by superimposing a lattice on the cells. The value at a lattice site (i,j) is σ if the site lies in cell σ. Each cell occupies multiple lattice sites and the connected set of lattice sites with the same index represents one cell. The evolution is MonteCarlo–Boltzmann, using Metropolis dynamics [21,22]. Cells rearrange diffusively to minimize the total effective free energy.

The CPM Hamiltonian describes the free energy resulting from the interactions among cells and between cells and their environment. Our Hamiltonian includes three terms

$$H = \sum_{(i,j),(i',j')} J_{\tau,\tau'}(\sigma(i,j),\sigma'(i',j'))(1-\delta_{\sigma(i,j),\sigma'(i',j')}) + \sum_{\sigma} \lambda_A(\tau)(A(\sigma)-A_t(\tau))^2 + \sum_{(i,j)} \mu(\tau) C_f(i,j)\ .$$

The first term describes the surface adhesion energy between cells and between cells and their environment. The sum is over (i,j) and (i',j') neighbors. We use the 20, 4th nearest neighbors. This range has lower anisotropy (an artifact of the technique which is not present in the biology) than 1st, 2nd, or 3rd-neighbor square lattices. τ is the cell type. We treat the environment, including the culture solution and substrate, as a single cell with $\tau = 0$, while all the biological cells are of type $\tau = 1$. $\sigma(i,j)$ is the index of lattice site (i,j). Sites with the same index define a cell. So, $J_{\tau,\tau'}(\sigma(i,j),\sigma'(i',j'))$ denotes the interaction energy between the neighboring sites (i,j) and (i',j'). We make each cell's surface energy a variable to reflect the increase in membrane-bound adhesion molecules in response to fibronectin. If $J_{11}(\sigma,\sigma') \neq J_{11}(\sigma',\sigma)$, we set $J_{11}(\sigma,\sigma') = J_{11}(\sigma',\sigma) = \min(J_{11}(\sigma,\sigma'),J_{11}(\sigma',\sigma))$. We also tested that using $J_{11}(\sigma,\sigma') = J_{11}(\sigma',\sigma) = \max(J_{11}(\sigma,\sigma'),J_{11}(\sigma',\sigma))$ (data not shown), did not critically affect the final configuration of the simulation.

The second term provides for the cells' resistance to compression. The actual cell area is $A(\sigma)$ and the target cell area is $A_t(\tau)$. The sum is over all cells with $\tau = 1$. $\lambda_A(\tau)$ acts as a Lagrange multiplier and governs the compressibility of the cell.

The third term describes the effect of preferential attachment of cells to fibronectin and the sum includes only the sites that lie within cells. $C_f(i,j)$ is the concentration of fibronectin at lattice site (i,j) and $\mu(\tau)$ is the unit strength of the fibronectin-binding. We make the simplest assumption, that all cells have the same value of μ. When a cell occupies a pixel (i,j) previously occupied by medium, the energy decreases by $\mu C_f(i,j)$. In the reverse process, the energy increases by $\mu C_f(i,j)$.

At each step we select a lattice site (i,j) at random and change its index from σ to σ' (where σ' is the index of an arbitrary lattice site from the first-order neighborhood) with Boltzmann probability, for a temperature $T > 0$,

$$P(\sigma(i,j) \to \sigma'(i,j)) = \begin{cases} \exp(-\Delta H/kT) & \text{if } \Delta H > 0, \text{ or} \\ 1 & \text{if } \Delta H \leqslant 0\ , \end{cases}$$

where ΔH is the energy gain produced by the change. Each such move corresponds to cell σ' displacing cell σ by one lattice site. T is a fluctuation temperature corresponding

to the amplitude of cytoskeletally-driven cell membrane fluctuations which we can measure experimentally from either the diffusion constant of a cell or the amplitude of its membrane fluctuations [23].

We use a 600×600 pixel square lattice and restrict the initial cell distribution to a circle in the middle. 600 pixels represent 3 mm in the experiment, setting the spatial scale to 5 μm/pixel. A typical limb-bud mesenchymal cell is approximately 15 μm in diameter when viewed as a flat two-dimensional disc. Therefore each cell occupies approximately 7 pixels. Making the cells larger or smaller (in lattice sites) would change the length and timescales (and the time to run the simulation) but would not change the qualitative behavior of the pattern.

In our chick limb micromass culture experiments, we plate out in a petri dish a 10 μl DMEM culture-medium suspension of single cells from the distal 0.3 mm of HH stage 24–26 chick wing or leg buds (see Ref. [24] for details). After 45 min, some of the cells settle and attach to the bottom of the dish, creating a 3 mm circle of cells. We then use 1 ml DMEM culture medium to flush away any unattached cells. Condensation takes place 18–36 h after plating. We change the medium once every 2 days. Five days after plating, we fix the culture and stain it with *Alcian Blue* to visualize the differentiated cartilage [24]. Depending on the initial cell density, the cartilage pattern varies from a mixture of stripes and dots (medium density -1.75×10^7 cell/ml) to spots only (low density -1.5×10^7 cell/ml).

4. Model and simulation

We propose the following model for precartilage mesenchymal condensation in limb chondrogenesis: mesenchymal cells produce nondiffusing fibronectin and deposit it onto the substrate. Cells execute a random walk biased by their binding more strongly to fibronectin than to the substrate (haptotaxis). Fibronectin–cell surface binding upregulates the production of cell–cell adhesion molecules such as N-cadherin, increasing cells' adhesiveness to each other. The pattern continues to evolve until the cell–cell and cell–ECM binding is so strong that the cells 'freeze' (i.e., attach irreversibly to the substrate or fibronectin).

The properties of the cells change during the experiment. Based on Ref. [11] we assume that the fibronectin production rate increases five-fold 6 h after plating (Fig. 1(A)). We assume that each cell has an internal phase parameter, with cells producing fibronectin during half of the 24 h phase-cycle, randomly initialized (Fig. 1(C)). The actual fibronectin production is the product of Figs. 1(A) and (C). The phase parameter distinguishes intracellular from intercellular and extracellular regulation of cell behavior. N-cadherin expression increases 12 h after plating [15] (24 h for N-CAM [16]). $J_{11}(\sigma)$ represents the effective density of the surface-adhesion molecules on the cell membrane. The more adhesion molecules, the smaller $J_{11}(\sigma)$. We choose the simplest assumption for the upregulation of cell adhesion by cell–fibronectin binding: the increase of each cell's number of adhesion molecules is proportional to the fibronectin the cell has seen, reflected in a decreasing $J_{11}(\sigma)$ (Fig. 1(B)). Visible condensation occurs 18–36 h after plating.

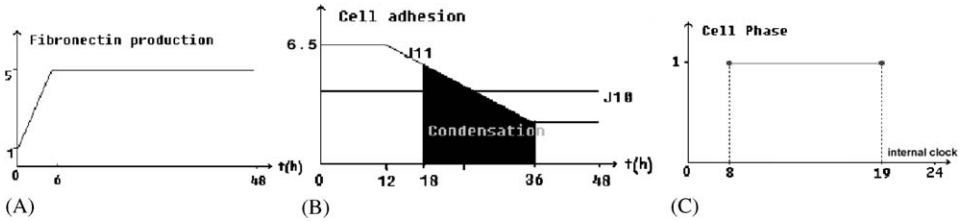

Fig. 1. (A) The fibronectin production of each cell. (B) The dependence of each cell's adhesiveness on the amount of fibronectin it has contacted. The shading shows the period of condensation. In the simulation we vary the slope by varying the initial J_{11} while fixing the final J_{11}. (C) Example of the fibronectin-producing phase of a cell: the sample cell produces fibronectin between 8 and 19 h.

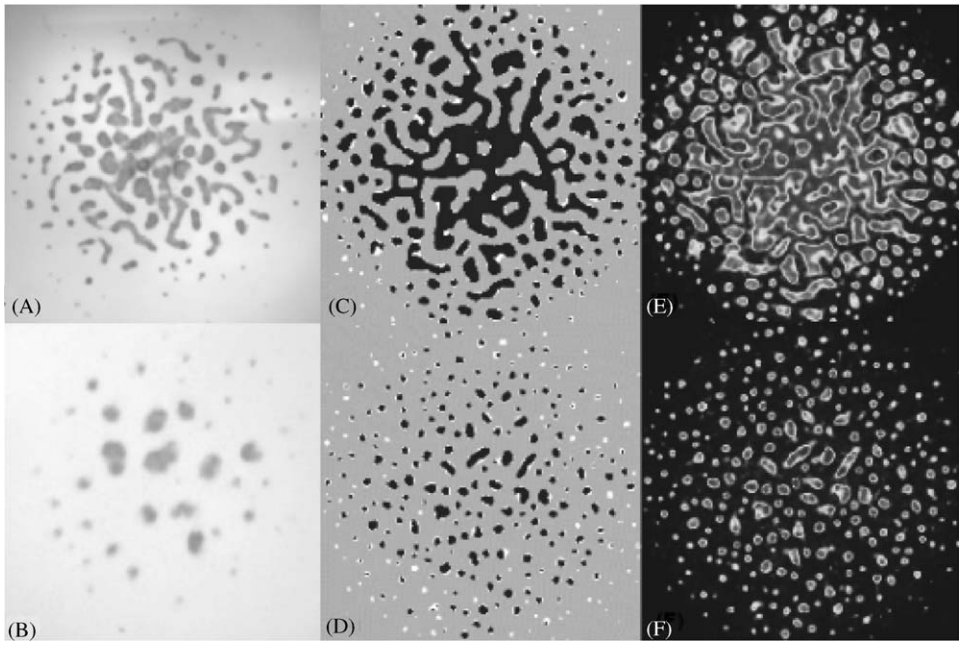

Fig. 2. (A) and (B). Experimental images of medium (A, 1.75×10^7 cell/ml) and low (B, 1.5×10^7 cell/ml) density condensations (redrawn from Ref. [25]). The white background represents both low levels of fibronectin and empty space. (C) and (D). In agreement with the experiment, the simulated cells form stripes and spots at medium densities (C, 35%) and only spots at low densities (D, 15%). (E) and (F) The distribution of fibronectin: the lighter-colored fibronectin peaks co-localize with the cell clusters. Parameters: $J_{11} = 6.5$ and $\mu = 0.25$.

5. Results

Precartilage mesenchymal condensations at medium and low culture density (Fig. 2) show very different morphologies. When the density is relatively high (Fig. 2(A)), the

condensations consist of both spots and 'finger-like' stripes, while dots form during low density condensation (Fig. 2(B)). In Fig. 2(C) we have a cell concentration of 35%, while in Fig. 2(D) the concentration is about 15%. Both cases show reasonable agreement with experiment. Figs. 2(D and E) show the fibronectin distribution beneath the cells. The parameters for the simulation are: $J_{11} = 6.5$ and $\mu = 0.25$.

If we consider the cells to be two-dimensional discs, the simulated densities seem much lower than in the experiments (as determined from the initial cell-suspension cell counts). However, three arguments suggest that the actual cell density on the bottom of the dish is much lower than the number counted in suspension. In the micromass experiment, massive cell death occurs in cells not in condensations [26] which decreases the "effective" cell density. Adding and changing the medium causes cell loss. Real cells can stretch vertically and crawl over each other. Thus the cell motility in our two-dimensional simulation is equivalent to the cell motility in the experiment only at lower density. Our three-dimensional simulations show that stripes and dots pattern arise at initial densities between 50% and 100% (reported elsewhere).

The clustering is robust: For each density, the same type of patterns occurs with minor modifications, given different values of μ and J_{11} (Fig. 3).

The cell density is the most significant parameter. At low density, spots always form while at high and medium densities, a mixture of dots and stripes forms, usually with stripes in the middle, surrounded by dots.

Spot-stripe selection depends on the relative rates of cluster coalescence and rounding and the total time before the cells freeze. Coalescence tends to produce elongated stripe-like clusters, while rounding produces spot-like clusters. The higher the cell density, the higher the rate of cluster coalescence. High density also lowers the cell mobility, slowing rounding, and reduces the time before cells bind irreversibly to the substrate. Thus high densities form stripes. When the cell density is low, coalescence is less frequent and cells have higher mobility and more time to diffuse before freezing, resulting in spots.

Due to experimental limitations, sometimes instead of the initial distribution of cells being uniform across the disk, it is nonuniform with higher density in the middle. We simulate this nonuniform case by using a gaussian distribution of cells, centered in the middle. This nonuniform distribution gives a bigger and more continuous sheet of condensation in the middle due to the higher local density, which reduces the cell motility.

μ represents the strength of cell–ECM binding. The smaller μ, the coarser the pattern. The bigger μ, the smaller the clusters and the shorter the wavelength. μ's effect on the pattern is the same as changing the fibronectin production rate. Faster fibronectin production corresponds to bigger μ.

J_{11} represents the strength of cell–cell adhesion. As the final J_{11} is fixed, the bigger the initial J_{11}, the stronger the upregulation of expression of cell adhesion molecules and the coarser the pattern. Cells can diffuse because of random membrane fluctuations and the diffusion constant decreases with increasing cell adhesion to other cells. Since the value of J_{11} remains positive during the simulation, our simulation has the defect that more adhesive cells, whose J_{11} is smaller, diffuse faster [27]. However, this incorrect hierarchy does not greatly affect the final pattern.

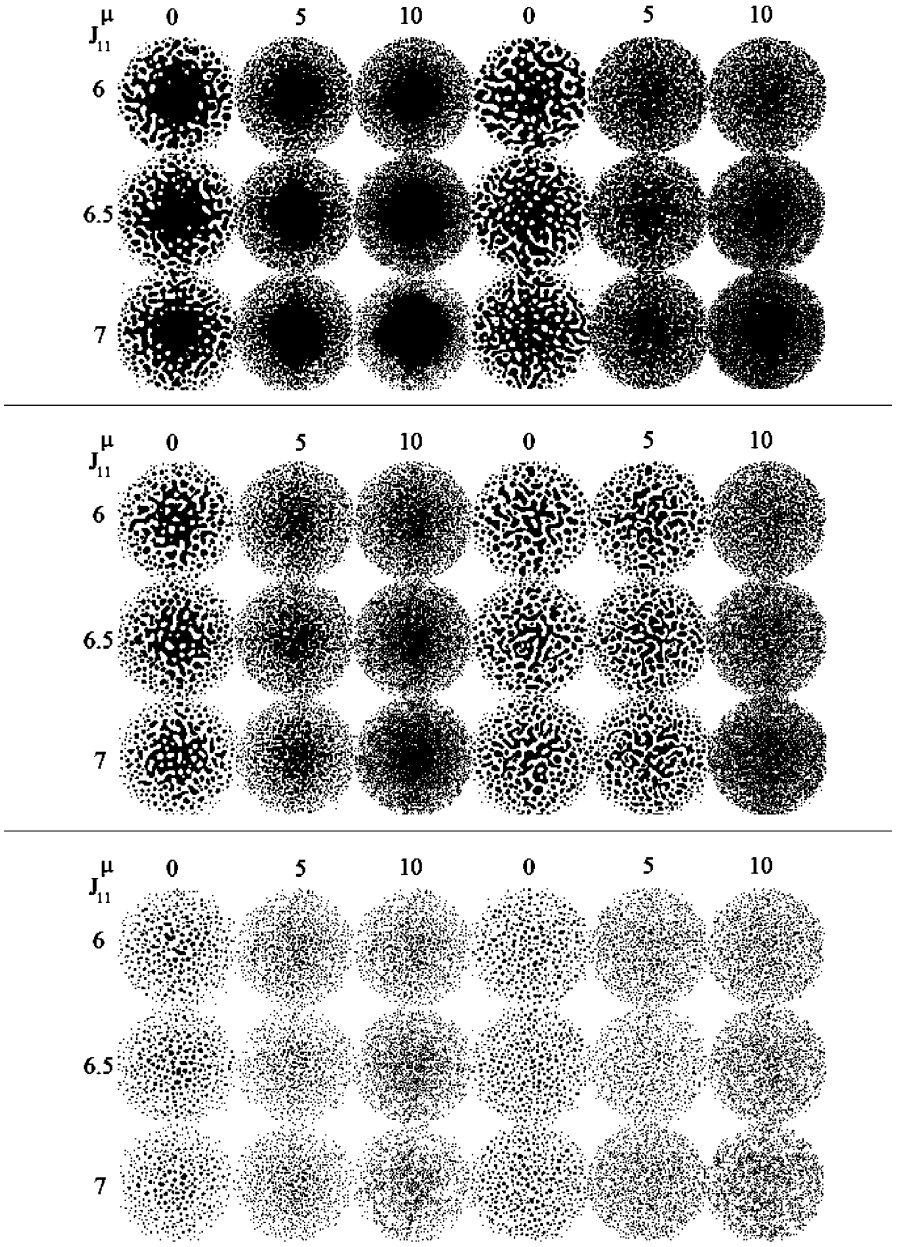

Fig. 3. Simulations with different combinations of parameters: high cell density (upper), medium cell density (center) and low cell density (lower). The first three columns on the left show simulations with a linear radial gradient in the initial cell distribution, and the last three columns on the right show simulations with a uniform initial cell distribution. The rows group simulations with the same initial J_{11}, and the columns group those with the same μ.

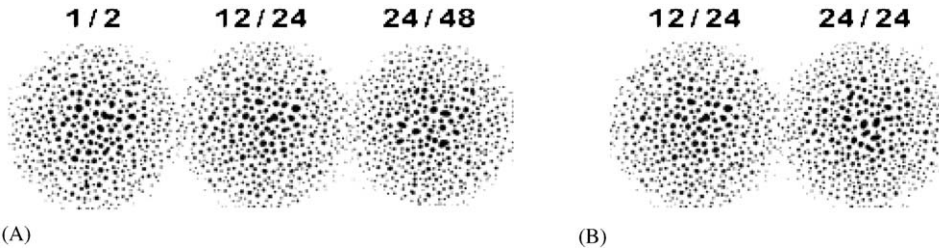

Fig. 4. (A) Comparison of patterns with different fibronectin production cycle lengths: 2, 24 and 48 h. (B) Comparison of patterns with different periods of fibronectin production during a cycle: 12 h out of a 24-h cycle and 24 h out of 24-h cycle.

The choice of period and duration of fibronectin production does not have a critical effect on the final pattern (Fig. 4(A)). Initially unsynchronized clocks and equal production and nonproduction phases are the simplest assumptions, but are not essential (Fig. 4(B)). Linking the phase parameter to the cell cycle is an interesting topic for further investigation [28].

We also tested the temperature dependence of our model (Fig. 5). Lower temperature corresponds to lower cell motility and leads to finer textured patterns at all cell densities.

In this paper, we restrict ourselves to qualitative descriptions of the parameter dependence of the patterns for a number of reasons. We have a limited number of experimental patterns for comparison and in these patterns we know whether the parameters increased or decreased, but not their exact values. Thus a detailed quantitative comparison will require further, more accurate experiments. Second, characterizing inhomogeneous spot-stripe patterns mathematically is notoriously difficult. While the human eye and brain immediately pick out features like mean spot size, spotness vs. stripeness, tortuosity and degree of cluster overlap, standard pattern analysis techniques like fourier transforms, periodograms, particle size distributions and wavelets cannot do so reliably. None of these methods works well for both spots and stripes and all require a manual identification of the spot-stripe boundary. We are currently working with Prof. Gemunu Gunaratne of the University of Houston to develop appropriate quantitative analysis techniques which we will present in a future paper.

6. Discussion

Our simulations show that spot and stripe patterns can result from a density dependent mechanism unrelated to the Turing mechanism. In our model, the instability arises from positive feedback in the fibronectin production. Cells tend to stay longer in regions with fibronectin, and hence become more adhesive and produce more fibronectin in those regions, further increasing the time the cells spend there. The wavelength grows continuously until cells stick and clusters cannot coalesce any more. Thus, our mechanism has no intrinsic wavelength. The duration and rate of coarsening together determine the final wavelength (higher temperatures lead to longer coarsening and hence

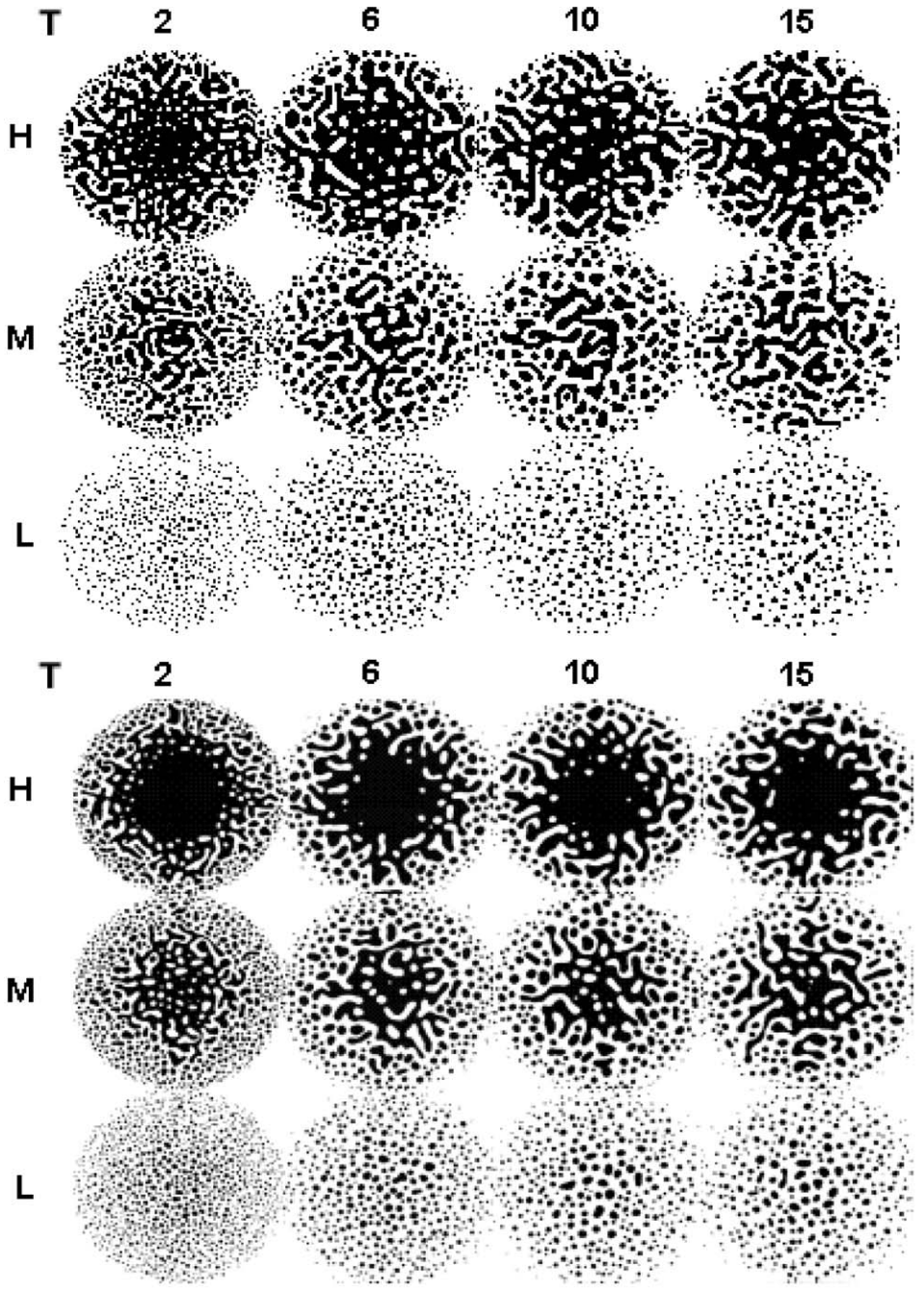

Fig. 5. The temperature dependence of the simulation. The top three rows show simulations with uniform initial cell distributions. The bottom three rows show simulations with a gradient in the initial cell distribution H: High density, M: Medium density, L: Low density, T: Temperature.

coarser and smoother patterns). High densities of cells lower the cells' motility—surface tension rounds clusters to reduce surface area, while coalescence tends to elongate them—and lead to more "stripe-like" patterns, while at low densities, cells move fast enough for the surface-energy driven rounding of clusters to dominate. The process has four time scales: the time till freezing, the rate of cluster coalescence, the rate of cluster rounding and the rate of cluster growth. In contrast, the wavelength of a Turing pattern depends on the diffusion constants of the morphogens and is independent of the cell density.

Adhesion can determine the size and number of condensations in vitro. We plan to extend our investigation of the mechanisms of limb chondrogenesis in vivo: differential adhesion of cells could determine the number and size of precartilage condensations from humerus to digits; the less adhesive cells in the proximal region would coarsen more and form one big humerus while the more adhesive cells in the distal region would form many smaller digits. Both in vitro and in vivo experiments support this hypothesis. For example, cell sorting experiments [29,30] suggest the presence of a gradient of cell adhesiveness in the proximo-distal axis of the limb. The proposed gradient of cell adhesiveness overlaps with the gradient of Hoxa gene expression [31,32]. Manipulation of Hoxa genes [20] alters both cell adhesiveness and bone shape. To study limb chondrogenesis in vivo, we need to describe mitosis, apoptosis, and chemotaxis in the CPM Hamiltonian. For example, limb mesenchymal cells also chemotax to the fibroblast growth factors (FGFs) that the *apical ectodermal ridge* (the AER, the protruding band of cells at the end of the limb running along where the tips of the fingers will be) secrets in intact limb [33]. Various limb segments are 'specified' early in limb development as distinct domains, with subsequent expansion of these progenitor populations mostly in the proximal–distal direction [34]. We can implement these mechanisms by letting cells divide and execute random walks biased not only by local cell–ECM binding but also by chemotaxis in the proximo-distal direction to FGFs from the AER. We can add new terms to describe other plausible mechanisms and study each mechanism individually by "turning off" other mechanisms as computational "knockouts."

One advantage of our model is that it involves only identified molecules: we know a fair amount about surface adhesion molecules and extracellular matrix. Most of the simulation parameters are experimentally measurable. For instance, Atomic Force Microscopy can directly measure the cell adhesiveness and cell–ECM binding strength. The cell size sets the spatial scale, while measuring the diffusion constant establishes the time scale. We can also refine the diagrams in Fig. 1 as additional data become available. Thus our cell–cell/cell–substrate adhesion model is able to duplicate many of the experimentally observed parameter dependencies of mesenchymal condensations. That such a simple mechanism which involves only known biological processes has been overlooked for so long is genuinely surprising. The mechanism need not apply only to biological cells but to any particulate material with changes in cell–cell and cell–substrate adhesivities. For example, if we make ΔJ_{10} a linear function of ΔJ_{11} we obtain labyrinths resembling those in magnetic domains (data not shown). It also functions in three dimensions and we are conducting simulations to study its three-dimensional properties.

Acknowledgements

Grants NSF-IBN-008365, NASA-NAG2-1619 and CAPES-Brazil. The authors are grateful to Stuart Newman for his experimental instruction and discussions about the biological aspects of the work, though his interpretation of the experiments differs from ours. We thank Mark Alber, Cornelis Weijer and Gemunu Gunaratne for critical reading and comments.

References

[1] L. Wolpert, Principles of Development, second ed., Oxford University Press, Oxford, 2001.
[2] S.F. Gilbert, Developmental Biology, seventh ed., Sinauer Associates, Inc., New York, 2003.
[3] N.A. Newman, H.L. Frisch, Dynamics of skeletal pattern formation in developing chick limb, Science 205 (1979) 662–668.
[4] A.M. Turing, The chemical basis of morphogenesis, Phil. Trans. Roy. Soc. B 237 (1952) 37–72.
[5] V. Castets, E. Dulos, J. Boissonade, P. De Kepper, Experimental evidence of a sustained standing turing-type nonequilibrium chemical pattern, Phys. Rev. Lett. 64 (1990) 2953–2956.
[6] J.D. Murray, Mathematical Biology, Springer, Berlin, 1989.
[7] S. Kondo, R. Asai, A viable reaction-diffusion wave on the skin of Pomacanthus, a marine angelfish, Nature 376 (1995) 765–768.
[8] B.K. Hall, T. Miyake, All for one and one for all: condensations and the initiation of skeletal development, BioEssays 22 (2000) 138–147.
[9] E.L. George, E.N. Georges-Labouesse, R.S. Patel-King, H. Rayburn, R.O. Hynes, Defects in mesoderm, neural tube and vascular development in mouse embryos lacking fibronectin, Development 119 (4) (1993) 1079–1091.
[10] N.A. Newman, J.J. Tomasek, Morphogenesis of connective tissues, in: W.D. Comper (Ed.), Extracellular Matrix, Molecular Components and Interactions, Vol. 2, 1996.
[11] W.M. Kulyk, W.B. Upholt, R.A. Kosher, Fibronectin gene expression during limb cartilage differentiation, Development 106 (1989) 449–455.
[12] C.M. Leonard, H.M. Fuld, D.A. Frenz, S.A. Downie, J. Massague, S.A. Newman, Role of transforming growth factor-beta in chondrogenic pattern formation in the embryonic limb: stimulation of mesenchymal condensation and fibronectin gene expression by exogenous TGF-beta and evidence for endogenous TGF-beta-like activity, Dev. Biol. 145 (1991) 99–109.
[13] T. Miura, K. Shiota, TGFbeta2 acts as an "activator" molecule in reaction–diffusion model and is involved in cell sorting phenomenon in mouse limb micromass culture, Dev. Dyn. 217 (2000) 241–249.
[14] M.Z. Moftah, S.A. Downie, N.B. Bronstein, N. Mezentseva, J. Pu, P.A. Maher, S.A. Newman, Ectodermal FGFs induce perinodular inhibition of limb chondrogenesis in vitro and in vivo via FGF receptor 2, Dev. Biol. 249 (2002) 270–282.
[15] S.A. Oberlender, R.S. Tuan, Expression and functional involvement of *N*-cadherin in embryonic limb chondrogenesis, Development 120 (1994) 177–187.
[16] R.B. Widelitz, T.X. Jiang, B.A. Murray, C.M. Chuong, Adhesion molecules in skeletogenesis: II. Neural cell adhesion molecules mediate precartilaginous mesenchymal condensations and enhance chondrogenesis, J. Cell Physiol. 156 (1993) 399–411.
[17] F. Monier-Gavelll, J.L. Duband, Cross talk between adhesion molecules: control of *N*-cadherin activity by intracellular signals elicited by betal and beta3 integrins in migrating neural crest cells, J. Cell. Biol. 137 (1997) 1663–1681.
[18] S. Dufour, A. Beauvais-Jouneau, A. Delouvee, J.P. Thiery, Differential function of *N*-cadherin and cadherin-7 in the control of embryonic cell motility, J. Cell. Biol. 146 (1999) 501–516.
[19] T. Miura, K. Shiota, Extracellular matrix environment influences chondrogenetic pattern formation in limb bud micromass culture: experimental verification of theoretical models, Anat. Rec. 258 (2000) 100–107.

[20] Y. Yokouchi, S. Nakazato, M. Yamamoto, Y. Goto, T. Kameda, H. Iba, A. Kuroiwa, Misexpression of Hoxa-13 induces cartilage homeotic transformation and changes cell adhesiveness in chick limb buds, Genes Dev. 9 (1995) 2509–2522.
[21] F. Graner, J.A. Glazier, Simulation of biological cell sorting using a two-dimensional extended potts model, Phys. Rev Lett. 69 (1992) 2013–2016.
[22] J.A. Glazier, F. Graner, Simulation of the differential adhesion driven rearrangement of biological cells, Phys. Rev. E 47 (1993) 2128–2154.
[23] J.C.M. Mombach, R.C. Raphael, M. Zajac, J.A. Glazier, Quantitative comparison between differential adhesion models and cell sorting in the presence and absence of fluctuations, Phys. Rev. Lett. 75 (1995) 2244–2247.
[24] S.A. Downie, S.A. Newman, Morphogenetic differences between fore and hind limb precartilage mesenchyme: relation to mechanisms of skeletal pattern formation, Dev. Biol. 162 (1994) 1955–1208.
[25] W. Zeng, G.L. Thomas, S.A. Newman, J.A. Glazier, A novel mechanism for mesenchymal condensation during limb chondrogenesis in vitro, in: V. Capasso, M. Ortisi (Eds.), Mathematical Modeling and Computing in Biology and Medicine: 5th Conference of the European Society of Mathematical and Theoretical Biology, Milan, 2002.
[26] M. Omi, M. Sato-Maeda, H. Ide, Role of chondrogenic tissue in programmed cell death and BMP expression in chick limb buds, Int. J. Dev. Biol. 44 (2000) 381–388.
[27] A. Upadhyaya, Thermodynamic and Fluid Properties of Cells, Tissues and Membranes, Ph.D. Dissertation, University of Notre Dame, 2000.
[28] K. Ohsugi, D.M. Gardiner, S.V. Bryant, Cell cycle length affects gene expression and pattern formation in limbs, Dev. Biol. 189 (1997) 13–21.
[29] A. Mochizuki, N. Wada, H. Ide, Y. Iwasa, Cell–Cell adhesion in limb-formation, estimated from photographs of cell sorting experiments based on a spatial stochastic model, Dev. Dyns. 211 (1998) 204–214.
[30] H. Yajima, K. Hara, H. Ide, K. Tamura, Cell adhesiveness and affinity for limb pattern formation, Int. J. Dev. Biol. 46 (2002) 897–904.
[31] C.E. Nelson, B.A. Morgan, A.C. Burke, E. Laufer, E. DiMambro, L.C. Murtaugh, E. Gonzales, L. Tessarollo, L.F. Parada, C. Tabin, Analysis of Hox gene expression in the chick limb bud, Development 122 (5) (1996) 1449–1466.
[32] S.A. Newman, Sticky fingers: hox genes and cell adhesion in vertebrate limb development, Bioessays 18 (1996) 171–174.
[33] S. Li, K. Muneoka, Cell migration and chick limb development: chemotactic action of FGF-4 and the AER, Dev. Biol. 211 (1999) 335–347.
[34] A.T. Dudley, M.A. Ros, C.J. Tabin, A re-examination of proximodistal patterning during vertebrate limb development, Nature 418 (6897) (2002) 539–544.